Cellulose (2023) 30:11845–11860
https://doi.org/10.1007/s10570-023-05597-8

ORIGINAL RESEARCH

Construction of 'wire-surface' conductive networks on cotton fabric for electromagnetic interference shielding, personal thermal management and infrared thermal camouflage

Biaobiao Yan · Yilei Gao · Bingjie Fan · Man Zhou · Ying Liu · Yuanyuan Yu · Bo Xu · Qiang Wang · Ping Wang

Received: 4 July 2023 / Accepted: 2 November 2023 / Published online: 10 November 2023

Abstract Although textiles decorated with electroactive materials have gained significant development in the field of wearable electronics and portable devices, the main issue is how to better exploit the synergy between conductive media for multi-scenario applications. Herein, we constructed a conductive network of 1D CNTs and 2D gallic acid-modified MXene (MG) alternating assembly of 'wire-surface' structure on the cotton fabric surface for wearable multifunctional personal protection. The introduction of gallic acid extended the lateral dimensions of MXene nanosheets, and the presence of CNTs protected MXene from oxidation and improved the binding of nanosheets to cotton fabric, contributing to an enhancement of the conductivity of the assembled fabric. Meanwhile, the conductivity of the assembled fabric remains stable after cyclic bending (1000 cycles) and nature storage (60 days). The assembled fabric could achieve more than 35 dB of electromagnetic interference shielding effectiveness (X-band) and outstanding infrared thermal camouflage performance. Moreover, low-radiation, *Joule* and solar heating are integrated to respond to the heating needs of complex scenarios and to achieve efficient utilization of energy. Based on its simple and scalable fabrication process, along with durability and comfort, the assembled cotton is expected to be promising candidates for multifunctional personal protective fabric.

Keywords Electroactive materials · Alternating assembly · 'Wire-surface' structure · Protective fabric

Introduction

More recently, with the continuous development and expansion of human working life style and field, it faces more and more external threats, such as electromagnetic radiation, low temperature and harsh environment. The development of personal protective fabrics, which can effectively avoid the body from being harmed by the outside in the course of activities, has been increasingly emphasized. The research of flexible electronic devices in the fields of electromagnetic interference (EMI) shielding (Wang et al. 2019; Su et al. 2023), human health monitoring (Takei et al. 2015), personal thermal management (Liu et al. 2018; Zhang et al. 2022) and human-machine interaction (Cao et al. 2018) has gained rapid developments. In general, flexible electronic devices are usually made of soft plastic substrates and conductive materials

Supplementary Information The online version contains supplementary material available at https://doi.org/10.1007/s10570-023-05597-8.

B. Yan · Y. Gao · B. Fan · M. Zhou · Y. Liu · Y. Yu · B. Xu · Q. Wang · P. Wang (✉)
Key Laboratory of Science and Technology of Eco-Textile, Ministry of Education, Jiangnan University, 1800 Lihu Avenue, Wuxi 214122, People's Republic of China
e-mail: pwang@jiangnan.edu.cn

directly composite, with simple processability, easy to industrialize and fast manufacturing. However, the soft plastic substrate is less compatible with the skin, especially when the body sweats, bacteria can easily grow between the skin and the substrate, causing serious discomfort to the body (Guo et al. 2023). In contrast, natural fiber are candidates for ideal substrates for flexible wearable devices because of their outstanding skin-friendliness, breathability, and inherent biocompatibility (Heo et al. 2018; Jin et al. 2019). However, it is still challenging to further explore the potential of conductive materials for multifunctional and multi-scenario applications while making rational use of flexible textile substrates.

Many electroactive materials such as conductive polymers (Cui et al. 2022; Allison et al. 2017), metal nanowires (Guo et al. 2021; Hsu et al. 2015), carbon nanotubes (CNTs) (Li et al. 2020; Yao et al. 2021), graphene (Ji et al. 2017; Zhao et al. 2020) and MXene nanosheets (Yan et al. 2022; Li et al. 2022) have been efficiently coated on textile surfaces by diverse strategies including in-situ polymerization, dip-coating, spraying, screen printing and vacuum-assisted deposition. Normally, conductive polymers such as polyaniline, polypyrrole and polythiophene can be obtained by catalytic oxidation with oxidants or enzymes, and dopants need to be added to obtain better conductivity. For the conjugated polymers, the complex processing procedures and poor chemical stability limit their wider applications. Metal nanowires can be spontaneously stacked and welded on the substrate surface with flexibility and high conductivity, but they also suffer from poor dispersion and the disadvantages of easy aggregation and oxidation (Gupta et al. 2016). The CNTs and graphene, both of which are carbon derivatives, have gained a lot of attentions and achieved more applications due to their excellent conductivity. Ghosh et al. used CNTs coatings and beaded fibers to weave smart fabrics for enhancing the mechanical and electrical properties of the flexible functional materials (Ghosh et al. 2023). In addition, they fabricated a carbonaceous coating to develop an intelligent cotton fabric with remarkable EMI shielding efficiency through the 'knife-over-roll' strategy (Ghosh et al. 2018). However, the poor water dispersibility and binding fastness limit their wider diffusion (Lee et al. 2018; Yang et al. 2018). MXene is the collective name for transition metal carbides, nitrides or carbonitrides, and is one of the newest members of the 2D materials family (Naguib et al. 2011). Among them, $Ti_3C_2T_x$-MXene as the outstanding representative has received the most extensive and intensive investigations. MXene nanosheets with excellent water dispersion can be obtained by selective etching of its precursor MAX phase (Alhabeb et al. 2017). Unfortunately, due to structural vacancies and atomic defects in MXene, when exposed to air or water, it tends to degrade rapidly by oxidation in a short period of time, eventually forming titanium dioxide (TiO_2) and amorphous carbon (C) (Lipatov et al. 2016). We previously reported a conductive fabric prepared by coating with MXene as a single electroactive medium, which showed good personal protection capabilities (Yan et al. 2022, 2023). However, the durability of a single electrically conductive material for complex environments is challenging, and the large-scale preparation of fabrics remains difficult. In summary, it is necessary to conduct an in-depth study of the physicochemical properties of conductive materials and to draw on the advantages of each material in a rational way to bring out their synergy. Based on the preparation of conductive textiles with stability and reliability, it is pressing to further develop their great potential to adapt to the needs of multi-scenario applications.

Here, we report a novel 'wire-surface' conductive network configuration of fabrics with stable and reliable multifunctional personal protection properties. One-dimensional 'wire' and two-dimensional 'surface' structures of CNTs and MXene were selected as electroactive raw materials for deposition on the surface of cotton fibers using a layer-by-layer alternating assembly strategy. The service stability of conductivity for the assembled cotton under cyclic bending-recovery and nature storage conditions was investigated. On this basis, the EMI shielding effectiveness of the composite fabric and the corresponding shielding mechanism are discussed. Moreover, integrated exploration of low-radiation heating, *Joule* heating and solar heating of textiles was also carried out. As a next-generation wearable smart protection product, we expect this multifunctional fabric to benefit society in the future.

Experimental section

Materials

The cotton woven fabric (CF) (180 g/m^2, thickness 0.272 mm) were purchased from Shanghai Textile

Industry Technical Supervision Institute. Ti_3AlC_2 (400 mesh, 98%) was supplied by Jilin 11 Technology Co. Hydrochloric acid (HCl, 36-38wt%) was obtained from Sinopharm Chemical Reagent Co. Lithium fluoride (LiF, 99.99%), gallic acid (GA, 99%) and carboxylated multi-walled carbon nanotubes (inner diameter, 5–10 nm, outer diameter, 10–20 nm) were provided by Shanghai Aladdin Reagent Co.

Preparation of assembled fabrics

MXene dispersions were prepared according to the previously reported method (Yan et al. 2021). Subsequently, the diluted MXene (3 mg/mL) was reacted with GA by hybridization at a mass ratio of 5:1 for 1 h, the hybridized dispersion was named as MG. Meanwhile, the carboxylated carbon nanotubes (CNTs) dispersion (3 mg/mL) was sonicated for 10 min to promote its dispersion. Next, one side of a CF (10×10 cm^2) was sprayed with alternating electroactive CNTs and MG dispersions. The operation of each cycle included spraying CNTs and MG dispersions separately for 30 s (0.1 mL/s) and drying under vacuum at 60 °C for 1 h, the final sample was named MG-Cm/CF (m represents the number of spraying cycles). In additon, as the controls, the fabric samples sprayed with CNTs, MXene and MG alone under the same conditions were prepared and named Cn/CF, Mo/CF and MGp/CF, respectively (n, o and p represent the number of spraying cycles, respectively).

Evaluation of thermal management performance

The reflectivity (r) and transmissivity (t) of fabrics in the wavelength range 200–2500 nm were obtained by a UV–Vis NIR spectrometer (Lambda 950, Perkin Elmer, USA) equipped with an integrating sphere. The absorptivity (a) of the fabrics at a specific wavelength (λ) and the average spectral absorptivity (A) in the range of 400–780 nm are calculated by Eqs. (1) and (2), respectively (Jose et al. 2014):

$$a = 1 - r - t \tag{1}$$

$$A = \frac{\int_{400}^{780} a(\lambda) i(\lambda) d(\lambda)}{\int_{400}^{780} i(\lambda) d(\lambda)} \tag{2}$$

where $a(\lambda)$ and $i(\lambda)$ are the spectral absorptivity and solar spectral irradiance (W m^{-2} nm^{-1}, ASTM standard G173-03), respectively.

A simulated sunlight xenon lamp (CEL-S500, Beijing Zhongjiao Jinyuan Technology Co., Ltd., China) was used as a light source to irradiate the fabrics, and the irradiation intensity could be controlled by adjusting the distance between the xenon lamp and the fabric surface. The *Joule* heating performance of the fabric was tested by a regulated DC power supply (TPR32-5 A, Antares, China). The low-radiation heating performance of fabrics was measured on a thermostatic silicone heating plate that simulates human skin. Specifically, a thermostatic silicone plate is covered with the fabric, and a K-type thermocouple is fixed between the heating plate and the fabric to detect the real-time temperature of the skin surface. A temperature detector (AS887, Sima, China) connected to a thermocouple was used to collect the temperature of a specific area of the sample. In addition, an IR thermal camera (Tis55, Fluke, USA) was used to acquire images of the surface temperature of the samples.

Characterization

The diluted CNTs, MXene and MG were dropped directly onto anodic aluminum oxide (AAO) (single-pass, pore center spacing 125 nm, pore diameter 80 nm, film thickness 150 nm) substrates, and dried under vacuum at 80 °C for 1 h. All samples were fixed on a metal table with conductive adhesive and sprayed with gold, and their micromorphology and element distribution were obtained using a scanning electron microscope (SEM) (SU8100, Hitachi Co., Japan) and an energy dispersive spectrometer (EDS) at an accelerating voltage of 4 kV, respectively. The UV–Vis spectra of hybrid dispersions was recorded by spectrophotometer (UV-1800, Shimadzu, Japan). The crystalline structure of assembled fabrics and lyophilized MXene powder was examined using an X-ray diffractometer (XRD) (D2 PHASER, Bruker, Germany). The measurement parameters of XRD were CuKα radiation ($\lambda=0.154$ nm), scanning rate 2°/min, and scanning range 4–60° (2θ). The spectral changes of fabrics in the range of 100–3200 cm^{-1} were recorded using a Raman spectrometer (inVia Reflex, Renishaw, UK) equipped with a 785 nm laser. A digital multimeter (VC890C, Victory Instruments,

China) was used to evaluate the resistance value of the fabric surface. The air permeability and water vapor transmission rate of fabrics were evaluated by air permeability meter (YG461E, Ningbo Textile Instrument Factory, China) and computerized fabric moisture permeability meter (YG601H-II, Ningbo Textile Instrument Factory, China), respectively. The EMI shielding effectiveness (SE) of the fabrics was examined (8.2–12.4 GHz, X-band) by vector network analyzer (Keysight, E5063A, Germany). The EMI shielding performance was provided according to the following Eqs (Iqbal et al. 2020):

$$R = |S11|^2 \tag{3}$$

$$T = |S21|^2 \tag{4}$$

$$A = 1 - R - T \tag{5}$$

$$SE_R = -10\log(1 - R) \tag{6}$$

$$SE_A = -10\log\left(\frac{T}{1 - R}\right) \tag{7}$$

$$SE_T = SE_R + SE_A \tag{8}$$

where S_{11} and S_{21} were the scattering parameters, R, T and A were the reflected, transmitted and absorbed power coefficients, respectively. Others, SE_R, SE_A, SE_T were represented reflected loss SE, absorbed loss SE, and the total SE, respectively.

Results and discussion

Fabrication and structure

Figure 1a illustrates a scalable layer-layer alternating assembly method for the fabrication of personal protection cotton fabrics with adjustable composition and structure. Firstly, carboxylated carbon nanotubes (CNTs) with well-dispersed properties were sequentially sprayed on the fabric surface to construct a conductive network with 1D 'wire' structure (C/CF). Subsequently, the polyphenolic hydroxyl structured gallic acid (GA)-hybridized MXene (MXene@GA, MG) nanosheet dispersions were prepared and sprayed on the C/CF surface. Based on the 1D structure, a highly conductive network with a 2D 'surface' structure was further constructed, and the result was designated as MG-Cm/CF (where m represents the spray cycles) and applied to a multifunctional personal protective fabric.

Figure 1b directly displays the microscopic morphology of CNTs with high aspect ratios (5–10 μm in length, and 15 nm in average diameter), which are flexible and bendable, facilitating the formation of interconnected conductive networks on the fiber surfaces. The morphological changes of MXene nanosheets before and after GA modification are shown in Fig. 1c, d. The MXene nanosheet dispersions were prepared by in situ synthesis of hydrofluoric acid to remove the aluminum layer from the precursor MAX phase Ti_3AlC_2, followed by centrifugal cleaning to neutrality, sonication and hand-shaking separation (Yan et al. 2021). The corresponding XRD patterns in Fig. S1 reflect the evolution of the crystalline structure from the MAX phase to monolayer or layer less MXene nanosheets. It can be seen from Fig. 1c that the monolayer or layer less MXene nanosheets have a large specific surface area and translucent. Interestingly, Fig. 1d shows that the transverse dimension of MXene nanosheets after the GA hybridization reaction, except for maintaining the original translucent structure, was significantly expanded from the previous 1–3 μm (Fig. S2). Due to the cross-linking effect of GA that can interconnect MXene nanosheets thorough their own polyphenol hydroxyls (Lee et al. 2020). It is noteworthy that this lateral size expansion is expected to improve the electrical conductivity after assembling the substrate.

Figure 1e indicates the migration of the extinction spectra of MXene nanosheet dispersions before and after GA hybridization, where 212 and 260 nm are the characteristic peaks of the organic small molecule GA benzene ring backbone, and 750 nm is the characteristic peak of MXene nanosheets (Yan et al. 2023). Clearly, the positions of the peaks did not change before and after the GA hybridization, indicating that the uniqueness of the MXene nanosheets was retained. In addition, the inset in Fig. 1e shows that the laser passing through the MG dispersion can produce a significant *Tyndall* effect, confirming the good dispersion of the MG nanosheets.

Raman spectroscopy was used to determine the differences in the surface groups of fabrics before and after modification with electroactive materials.

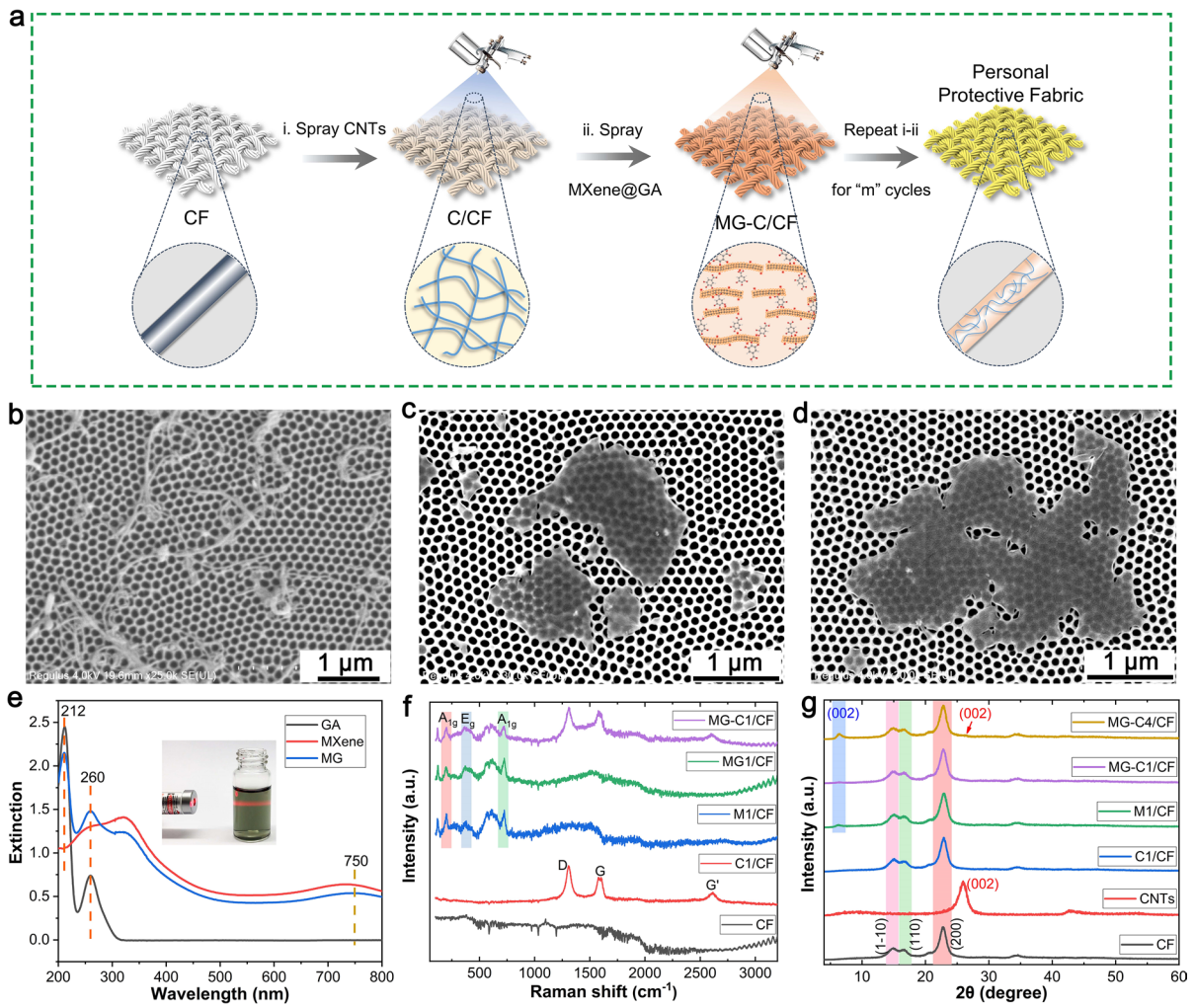

Fig. 1 **a** Schematic of fabrication of personal protective fabric. The SEM images of **b** CNTs, **c** MXene and **d** MXene@GA (MG) nanosheets. **e** Extinction spectra of samples (the illustration shows the laser passing through the MG dispersion). **f** Raman spectra and **g** XRD pattern of samples

Figure 1f reveals that the characteristic peaks of A_{1g}, E_g and A_{1g} were detected at 200, 370 and 720 cm^{-1} for the assembled fabrics, which correspond well to the lamellar vibrations of Ti, C and T_x, the vibrational stretching of oxygen atoms on the Ti surface, and the in-plane and out-of-plane vibrations of carbon on the MXene surface, respectively (Sarycheva et al. 2020). Furthermore, G′, G and D bands representing CNTs were observed on both C1/CF and MG-C1/CF surfaces (Cai et al. 2018). In summary, the obtained results illustrate the successful assembly of MXene and CNTs on the cotton surface. XRD was further used to trace the changes in the crystalline structure of the assembled fabrics, and the results are shown in Fig. 1g. Compared to the original CF, the assembled cotton fabrics still retain the cellulose (1–10), (110) and (200) crystalline planes, implying that the structure of the fabric was not evidently affected by the assembly behavior. MG-C4/CF exhibited the typical characteristic peaks at approximately 6.8° and 27.1° for (002) crystalline planes representing MXene and (002) crystalline planes for CNTs, which is consistent with the results of Raman spectral analysis.

Micromorphology of fabrics

To construct a conductive network with tunable compositions and structures on the fabric surface, an efficient and scalable layer-layer assembly spraying strategies was employed. From Fig. 2a and b, the original CF surface is smooth and neat. Notably, the assembled C/CF produced more fine villi on the surface (Fig. 2c, d), which is a direct evidence of the efficient deposition of 1D CNTs on the substrate. Furthermore, after cyclic layer-layer assembly, the MG-C4/CF microscopically shows an impressive number of deposits (Fig. 2e, f), narrow gaps between the cotton fibers are filled and the adjacent fibers are bridged, constructing homogeneous networks of electroactive coatings. In addition, Fig. 2g displays that the content of the characteristic element Ti on the MG-C4/CF surface is close to 30%, indicating that the deposit contained a large amount of 2D $Ti_3C_2T_x$ MXene.

The cross-sectional microscopic image of MG-C4/CF in Fig. 2h reveals that a remarkable coating is assembled, and it is perfectly integrated with the fibers on the surface of the substrate. Further, the EDS images clearly indicate that C and O elements are uniformly distributed over the entire cross-section of the fabric, while Ti elements are mainly concentrated in its upper layers (Fig. 2i). This is due to the fact that the original CF is mainly composed by C and O elements, while the Ti element is only from $Ti_3C_2T_x$ MXene. In addition, the front and back photographs of the assembled fabrics (Fig. S3) show that the conductive coating was mainly concentrated on the sprayed surface with little penetration to the other side, which ensured the efficiency of the utilization of

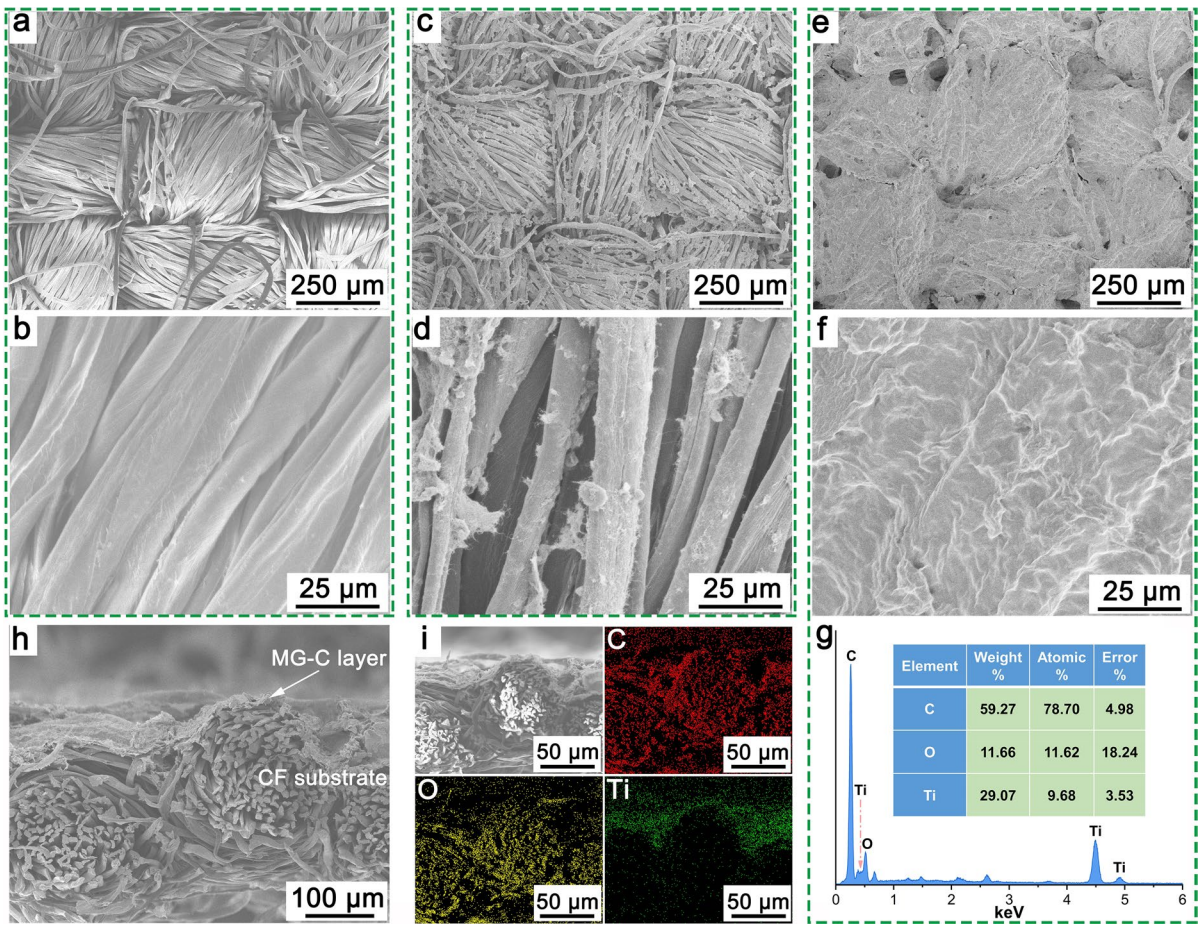

Fig. 2 The SEM images of **a**, **b** CF, **c**, **d** C/CF, and **e**, **f** MG-C4/CF. **g** Elemental mapping spectrum and contents of MG-C4/CF. **h**, **i** Cross-sectional SEM and EDS images of MG-C4/CF

the electroactive medium. As a result, a conductive coating network with a 'wire-surface' structure created on the cotton surface was demonstrated, and it is expected to play a unique role in the field of functional fabrics.

Conductivity and wearability

Each component plays a crucial role in the process of assembling coatings for the construction of 'wire-surface' surface on the fabrics. Therefore, the suitable combination of CNTs and MXene and the spraying amount on the fabric surface were explored. From Fig. 3a, the average resistance value per cm of C1/CF, M1/CF and MG1/CF were 121.5, 2.1 and 1.3 kΩ for just assembling a single cycle, respectively. This is because that 2D 'surface' MXene nanosheets are easier to form smooth conductive pathways when stacked compared to the 1D 'wire' structure of CNTs. In addition, combining the data in Fig. S4, it can be seen that the sample of MG/CF exhibits a decrease in the resistance compared to M/CF due to the increased lateral size of the nanosheets, which is consistent well with the analytical results in Fig. 1d. It is gratifying to note that the resistance value of MG-C1/CF (MXene 0.084 mg/cm^2, CNTs 0.084 mg/cm^2) can be reduced to 0.6 kΩ, indicating that the conductivity of the prepared fabrics can be significantly improved when the 'wire-surface' combination was employed. Furthermore, the resistance of MG-Cm/CF was gradually reduced by increasing the spraying assembly cycles (Fig. 3b). Among them,

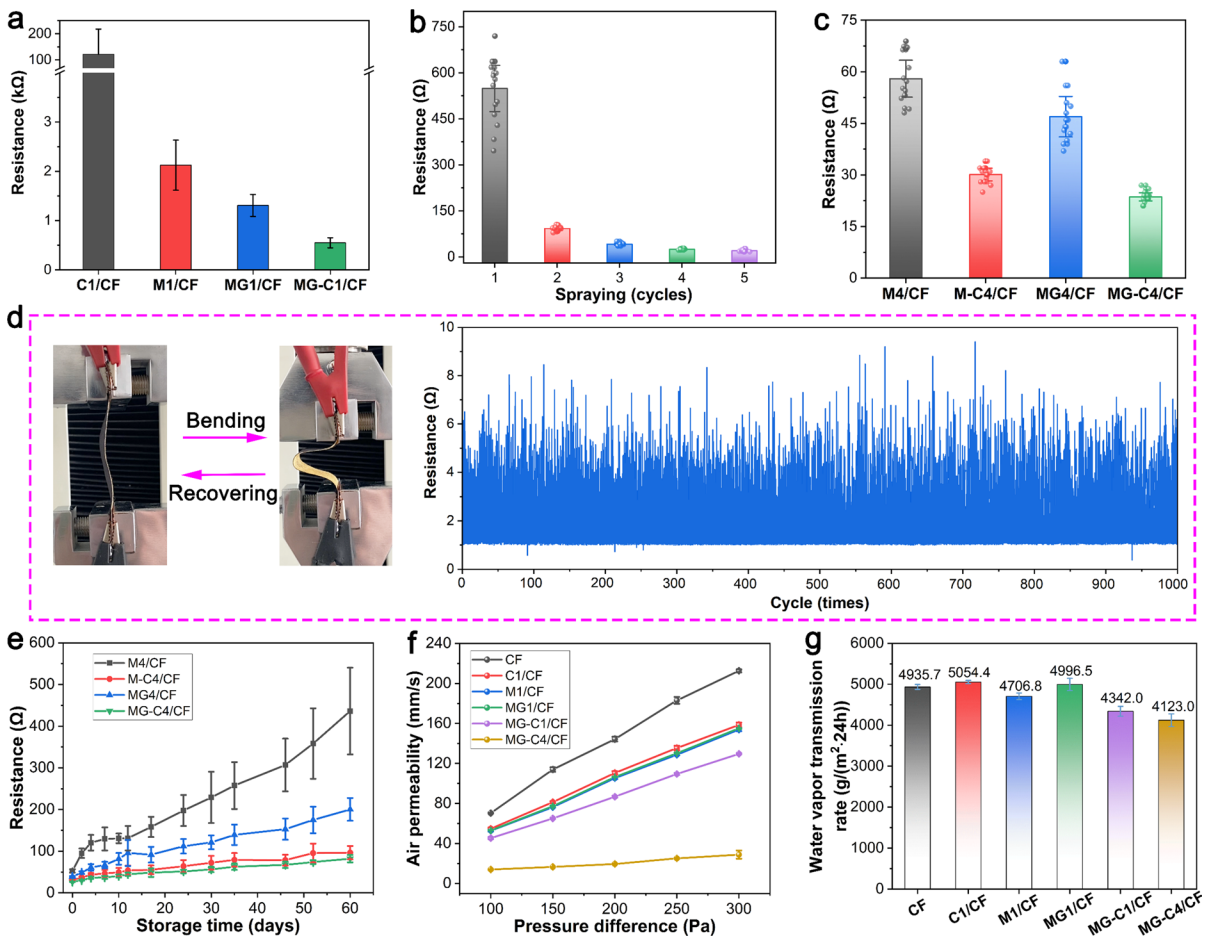

Fig. 3 Conductivity of **a** the comparison sample (spraying one cycle), **b** the spraying cycle and **c** the comparison sample (spraying four cycles). Effects of **d** bending-recovering and **e** natural storage on the conductivity of fabrics. **f** Air permeability and **g** water vapor transmission rate of fabrics

the resistance values decreased to 24.6 and 20.1 Ω after four (MXene 0.336 mg/cm^2, CNTs 0.336 mg/cm^2) and five (MXene 0.42 mg/cm^2, CNTs 0.42 mg/cm^2) assembly cycles, respectively, which indicates that better conductivity of the composite fabric was achieved after four cyclic assembly. In addition, as depicted in Fig. 3c, the sample of MG-C4/CF also has excellent conductivity compared to the other three comparison samples when the number of control spraying cycles is equal. Based on the above-mentioned discussion, four cycles of spraying assembly were selected for preparation of the MG-C4/CF in the following work.

The service stability of conductive fabrics is a critical factor in realizing their practical application potential. The bending resistance of the MG-C4/CF's conductivity was examined and the results are shown in Fig. 3d. After being subjected to 1 000 bending-recovering cycles, the surface resistance of the fabric remained essentially unchanged (10 Ω), proving its excellent flexible bending performance. It is well known that MXene is susceptible to oxygen and water attack in the natural environment, easily causing a dramatic decrease of its conductivity. For this purpose, the resistance values of the assembled fabrics were examined after a period of storage in the natural environment, and the results are presented in Fig. 3e. Obviously, the resistance of M4/CF increases dramatically (from 60 to 450 Ω) after 60 days of storage. In contrast, the sample of MG4/CF exhibited a slow increase in resistance, which was attributed to the phenolic hydroxyl structure of GA that had a scavenging effect on free radicals and retarded the oxidation of MXene nanosheets. Satisfactorily, both M-C4/CF and MG-C4/CF exhibit excellent storage stability, maintaining their resistance values within 100 Ω. This can be attributed to the scavenging of free radicals by the bent sp^2-hybridized framework in the CNTs (Lucente-Schultz et al. 2009). The wearing comfort for the conductive fabrics was explored. From Fig. 3f, the decrement of air permeability for the sample of MG-C4/CF was more remarkably compared to that of the original CF, which is due to the large number of electroactive media deposited on the fiber surface, blocking the free entry and exit of air. Importantly, the moisture vapor permeability of the MG-C4/CF is almost at the same level as that of the original CF (Fig. 3g), implying that it meets the requirement for daily use without feeling stuffy.

Electromagnetic interference shielding performance

The frequent use of portable electronic devices brings potential electromagnetic (EM) radiation pollution problems, so that human safety faces a serious challenge. MG-C4/CF have excellent conductivity and are expected to play a significant role in the field of EM interference (EMI) shielding. From Fig. 4a, b, the EMI total shielding efficiency (SE_T) of fabrics with different combinations or assembly cycles in the X-band frequency range of 8.2–12.4 GHz shows large differences. Specifically, CF, C1/CF, M1/CF, MG1/CF, and MG-C1/CF exhibited lower EMI SE_T due to electrical insulation or larger resistance values. In contrast, the EMI SE_T for MG-C4/CF reached approximately 20 dB, indicating its encouraging ability to shield 99% of EM waves. In particular, the thickness of MG-Cm/CF increased from 0.293 to 0.325 mm with the increase of the assembly cycle 'm', which indicates a large amount of electroactive medium deposition on the surface of the cotton fabric. Correspondingly, the EMI SE_T of the fabric also shows an increasing trend, but the difference between MG-C4/CF and MG-C5/CF is not significant, which is consistent well with the test results in Fig. 3b.

Moreover, the EMI SE_T, absorbed loss (SE_A), and reflected loss (SE_R) of MG-C4/CF with different number of folded layers were also analyzed. According to the results shown in Fig. 4c, the SE_A of the fabric increases significantly with the increase of the number of layers, while the SE_R remains basically the same. When the number of folded layers is four, the SE_T can reach more than 35 dB, showing excellent EMI shielding performance. Among them, the absorption ratio of electromagnetic waves (SE_A/SE_T) shows that the absorption ratio of textiles to EM waves gradually increases with the increase of the number of folded layers (Fig. 4d), which indicates that absorption plays a key role in the attenuation of EM waves.

The EMI shielding mechanism of textiles can be analyzed by calculating the *S*-parameters. Figure 4e displays the average values of the transmission (*T*), reflection (*R*) and absorption (*A*) power coefficients of the textile. It can be seen that *R* is always greater than *A* and *T*, which suggests that reflection plays a dominant role in EM wave attenuation. Figure 4f illustrates the specific process of EMI shielding of MG-C4/CF. A beam of high-energy incident EM waves intrudes

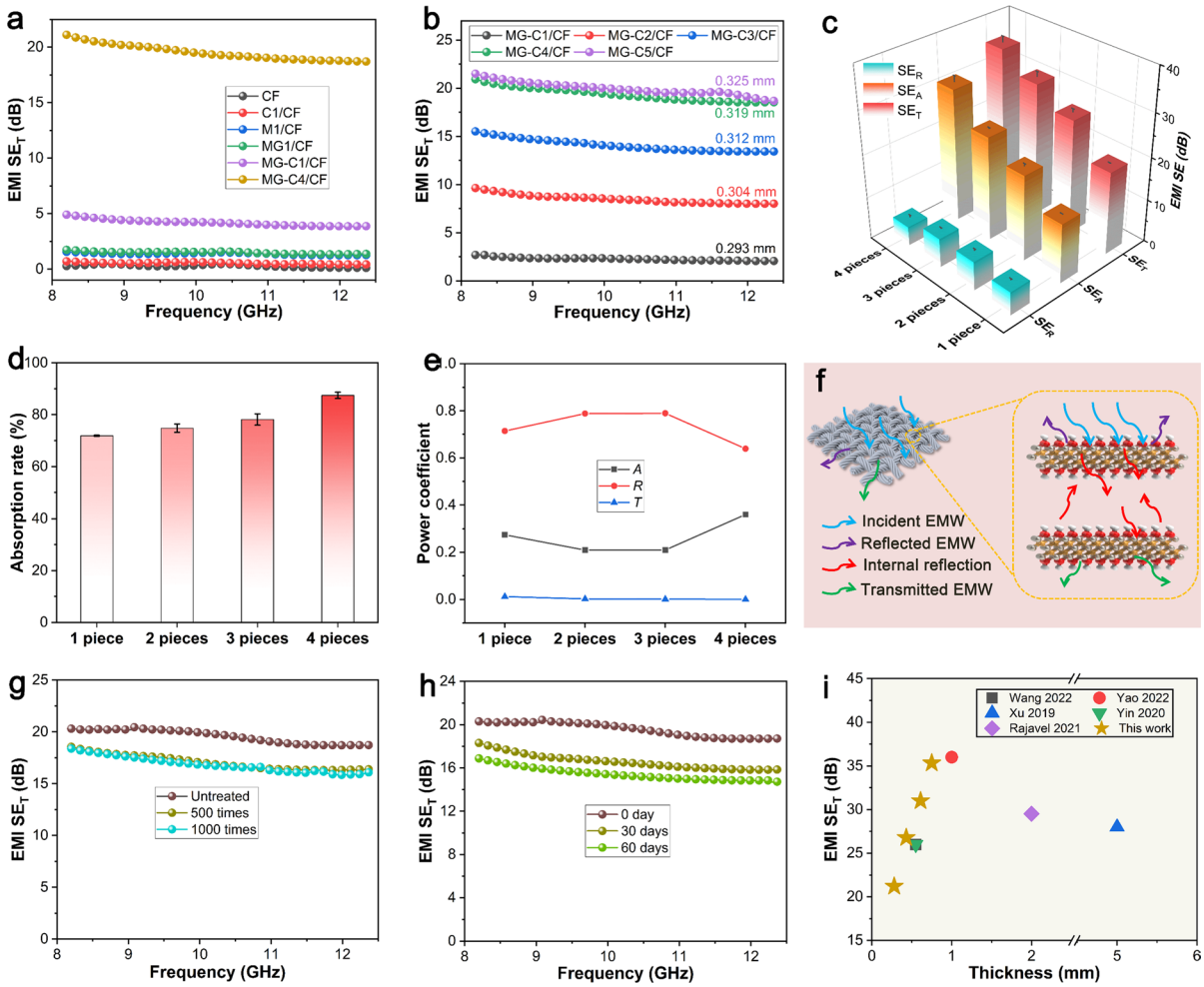

Fig. 4 **a** EMI SE$_T$ curves of different fabrics. Effect of **b** assembly cycle and **c** folded layers on the EMI SE$_T$ of fabric. **d** Absorption shielding ratio, **e** average EMI shielding coefficient and **f** EMI shielding mechanism of MG-C4/CF. Effect of **g** bending-recovering cycles and **h** natural storage times on the EMI SE$_T$ of MG-C4/CF. **i** Comparison of EMI SE of the MG-C4/CF with the previously reported works

on the outer surface of the fabric, forcing some of the radiated waves to be reflected immediately due to the superior free electron effect of the MXene nanosheets. The remaining radiated waves enter the nanosheet layer and are reflected and consumed in a continuous cycle, eventually being dissipated in space as heat.

The durability of the EMI shielding performance for the sample of MG-C4/CF was further evaluated. Notably, after enduring 1000 bend-recovery cycles, the fabric retains nearly 90% of its EMI SE$_T$ (Fig. 4g). In addition, the EMI SE$_T$ value is retained at more than 85% after 60 days of storage in a natural environment (Fig. 4h), indicating the remarkable service stability of MG-C4/CF. Highly EMI SE$_T$ with small thickness is the core element of a perfect EMI shielding material. The main indicators of EMI shielding of MG-C4/CF were compared with the recently reported works and were found to have significant advantages (Fig. 4i) (Wang et al. 2022; Yao et al. 2022; Xu et al. 2019; Yin et al. 2020; Rajavel et al. 2021).

Solar heating performance

With the rapid global economic and social development, the number of people is growing, leading to an increasing demand for energy. And fossil fuels, as non-renewable energy sources, are facing increasing depletion. Therefore, the development of sustainable, green and clean solar energy is of utmost importance. MXene ($Ti_3C_2T_x$), a transition metal carbide with a metal-like nature of local surface plasmon resonance (LSPR) effect, has been shown to have a high absorptivity in the solar spectrum (Li et al. 2017; Gao et al. 2019). As a functional material for photothermal conversion, it is expected to play a major role in the efficient utilization of solar energy.

The absorptivity (a) of fabrics in the UV to NIR wavelength range was obtained by testing their transmissivity (t) and reflectivity (r). From Fig. 5a, b and Fig. S5, the fabrics assembled by both CNTs and MXene exhibit low r, t and high a in the UV-visible-NIR wavelength range. Furthermore, the average a of CF, C1/CF, M1/CF, MG1/CF, MG-C1/CF and MG-C4/CF in the visible wavelength range of 400–780 nm was calculated to be 0.014, 0.816, 0.878, 0.873, 0.903 and 0.889, respectively. It can be found that the MG-C1/CF assembled by CNTs and MXene show the strongest spectral absorptivity, while the a

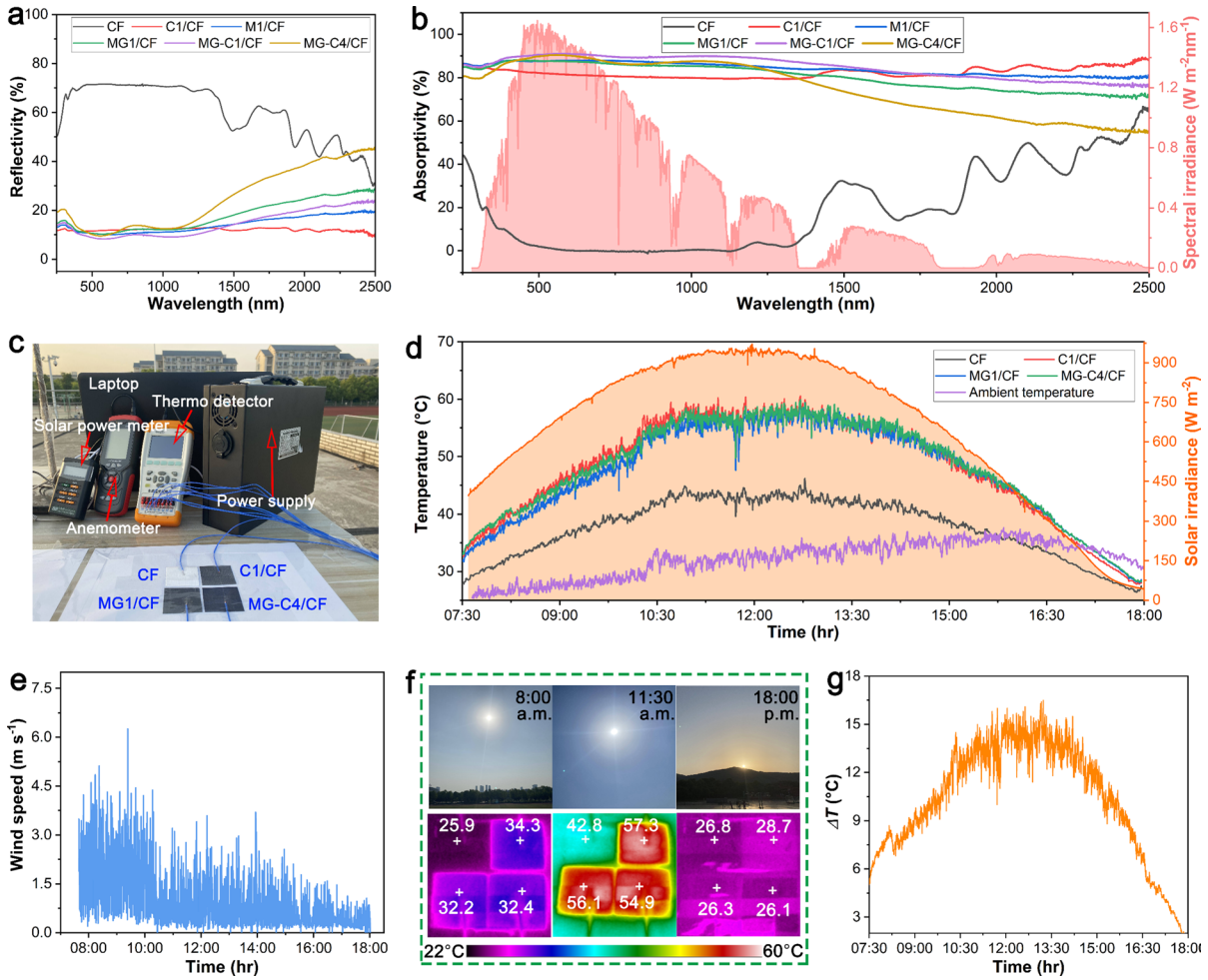

Fig. 5 Measured **a** reflectivity and **b** absorptivity of the fabrics from UV to NIR wavelengths. **c** Physical photograph of the measure device in an outdoor environment (May 14, 2023, 120°30′ E; 31°57′ N). **d** Temperature of the surface of the fabrics, and **e** the ambient wind speed. **f** Physical photograph of weather conditions (8:30, 12:00 and 16:30) and IR thermal photos of fabrics. **g** Surface temperature difference between MG-C4/CF and CF

of MG-C4/CF after multiple assemblies decreases rather than continues to increase. This is due to the formation of a thicker electroactive coating on the cotton surface after multiple cycles of assembly, resulting in a slight increase in spectral r, which in turn affects the final a.

The actual solar heating performance of the fabric was tested on May 14, 2023. Figure 5c displays the solar power meter, anemometer, thermometer with thermocouple attached, mobile power supply and laptop computer used for the experiment to record real-time solar power, wind speed, fabric surface temperature, provide experimental power and collect experimental data, respectively. Real-time temperature measurements were carried out at the experimental site (120° 30′ E, 31° 57′ N, Jiangnan University Northwest Soccer Field) throughout the day (7:30–18:00) and the collected results are presented in Fig. 5d. The real-time surface temperatures of C1/CF, MG1/CF and MG-C4/CF were all much higher than the original CF under sufficient sunlight irradiation, which is consistent with the test results in Fig. 5b. Under clear weather and breeze (Fig. 5e), the peak surface temperature of MG-C4/CF was 59.5 °C, which was 16.1 and 43.3 °C higher than the CF and ambient temperature, respectively.

Figure 5f exhibits the weather conditions on the day of the test and the corresponding infrared (IR) images of the fabric surface temperature. The surface temperatures of C1/CF, MG1/CF and MG-C4/CF were uniformly distributed under solar irradiation. At 11:30, the temperatures of the three samples detected by IR images were 57.3, 56.1 and 54.9 °C, respectively. Notably, the IR detection temperatures of MG1/CF and MG-C4/CF exhibit partial differences from the real-time temperatures collected by thermocouples, which may be due to the inherent low IR emissivity of MXene nanosheets that impairs the detection of heat (Li et al. 2021). In addition, the surface temperature difference (ΔT) between MG-C4/CF and CF consistently exceeded 10 °C during the 10:30–15:00 time period (Fig. 5g), indicating its excellent solar heating performance.

Personal thermal management

Besides, with a resistance value of 24.6 Ω, MG-C4/CF have excellent *Joule* heating performance, which can be used as a supplement in the face of complex heating environments. Figure 6a displays the *Joule* heating performance of the MG-C4/CF at different driving voltages. The temperature of MG-C4/CF surface can reach 19.8, 29.5, 44.5, 67.4, 96.9 and 131.2 °C after applying 2, 4, 6, 8, 10 and 12 V safety voltages, respectively. However, the photographs captured by the infrared camera revealed that the surface temperature of the fabric was significantly lower than the actual measured value (Fig. 6b), due to the low IR emissivity of MXene. Encouragingly, the *Joule* heating performance of MG-C4/CF is sensitive and adjustable, with a linear relationship between the surface temperature value and the load voltage U^2 (Fig. S6a). While switching the load voltage from 6 to 8 V, its surface temperature also changes from 47.5 to 67.6 °C correspondingly to obtain the needed heating temperature (Fig. 6c). The maximum value of its surface temperature can reach near 68 °C for 10 cycles of turning on and off the circuit at a voltage of 8 V (Fig. S6b). Importantly, Fig. 6d displays that the saturation temperature values of MG-C4/CF remain essentially constant under prolonged heating conditions, indicating a safe and reliable heating performance that avoids the risk of potential high-temperature burns. In addition, Fig. S6c shows the practical wearability of the MG-C4/CF, which can be fixed on the fingers or wrist to continuously provide a steady flow of heat to the body.

Based on the low IR radiation properties of MXene, we tested the warming properties of the fabric in a relatively constant temperature (25 ± 0.5 °C) room by means of a homemade experimental setup. A silicone heating plate connected with a DC power supply was used to simulate human skin to generate heat to simulate metabolic heat production. Fabrics are covered on the surface of the heating plate with K-type thermocouples fixed in the middle, and the temperature is recorded in real time when covered by different fabrics. From Fig. 6e, after 30 min, the "skin" temperature covered by MG-C4/CF reached 35.0 °C, which is 2.1 and 4.5 °C higher than the original CF and bare skin, respectively, indicating its remarkable low-radiation heating performance.

Subsequently, the different heating modes are integrated. Firstly, we have combined passive low-radiation heating and active *Joule* heating. By covering the MG-C4/CF and adjusting the load voltage (4 or 6 V), the surface temperature of the "skin" is precisely regulated (Fig. 6f). After covering the MG-C4/

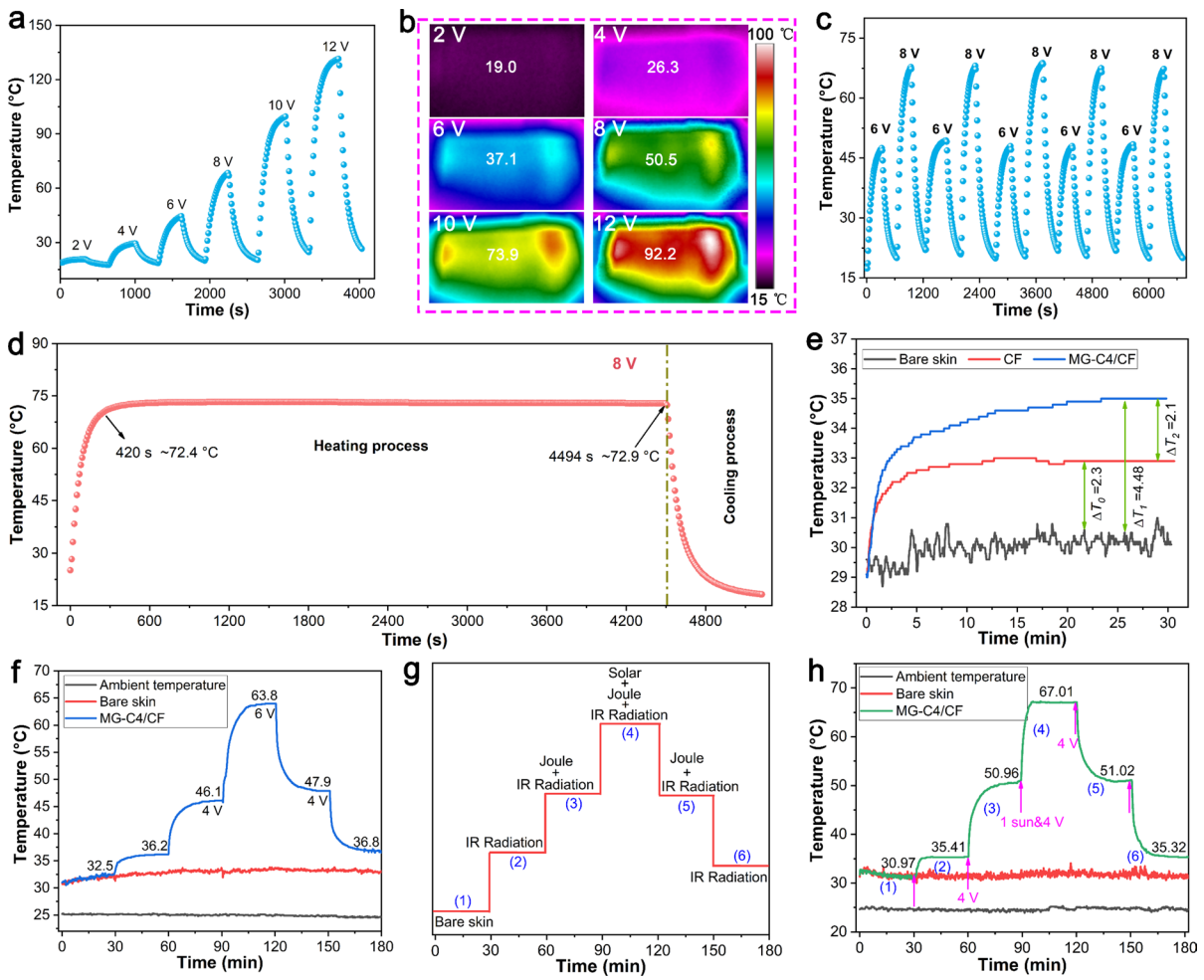

Fig. 6 Surface **a** real-time temperatures and **b** saturation temperature IR images of MG-C4/CF at different voltages. **c** Temperature variation curve at an alternating voltage. **d** Long-term heating test at 8 V. **e** Real-time temperature of the artificial skin covered with different fabrics (room temperature maintained at 25 ± 0.5 °C). **f** Dual heating mode of radiation heating and *Joule* heating in indoor environment. **g** Flexible switching procedure for radiant heating, *Joule* heating and solar heating modes. **h** Real-time temperature profile in the heating mode flexible switching program

CF, its temperature value can be increased to 36.2 °C. Then, by continuously loading 4 and 6 V, its surface temperature can reach 63.8 °C, which is much higher than the bare skin temperature (32.5 °C) in non-heated mode. Further, guided by the procedure of flexible switching of heating modes in Fig. 6g, we explored the synergistic effects of the combination of low-radiation heating, *Joule* heating and solar heating. In particular, the solar heating mode uses a simulated daylight xenon lamp to irradiate the surface of the fabric to obtain a steady source of sunlight radiation. Before, we investigated the warming behavior of fabrics under simulated daylight xenon irradiation. Figure S7 indicates that the surface temperature of the fabric becomes larger with increasing irradiation intensity in a linear correlation. When the irradiation intensity was maintained constant, the surface saturation temperature of the fabrics showed consistency regardless of the long time, or cyclic irradiation (Fig. S8, 9), indicating the stable controllability of the photothermal properties.

From Fig. 6h, the real-time temperature of the simulated skin surface was recorded when the three heating modes were switched. The surface temperature of the "skin" can reach 35.41, 50.96 and 67.01 °C in sequence with the addition of the MG-C4/CF cover,

4 V load and one sun irradiation daylight program. Subsequently, we withdrew the irradiation of simulated daylight and the surface temperature of the fabric was reduced to 51.02 °C. The supply of voltage was then stopped and its surface temperature was continuously reduced to 35.32 °C. The above results indicate that MG-C4/CF can provide enough clean thermal energy to effectively heat the body and enable precise thermal comfort for the body in a variety of situations as required. Therefore, in the condition of flexible combination of three heating modes, it can realize heating in all-weather and multi-scene modes, which is a very important feature of future personal precise thermal management fabrics.

Infrared thermal camouflage

Infrared (IR) thermal camouflage is a technique for blocking or attenuating thermal radiation in the mid-infrared band of 7–14 μm emitted by objects with temperatures above absolute zero (Salihoglu et al. 2018). With an ultra-low mid-infrared emissivity of 0.19, MXene-based film materials exhibit excellent IR thermal camouflage potential (Li et al. 2021). By assembling MXene more on the surface of fabric, it is expected to play a key role in the field of human IR thermal camouflage.

The fabrics were attached to a graphite heating plate with adjustable temperature, and the temperature distribution images of the fabrics surface were captured with an IR thermal camera while increasing the temperature of the heating plate. Figure 7a shows that at different set temperatures, CF and C1/CF exhibit similar detection temperatures to the surface of the heating plate, while the detected temperatures of M1/CF, MG1/CF, MG-C1/CF and MG-C4/CF differ significantly from that of the heating plate. Obviously, the MG-C4/CF presents the lowest detection temperature, and the temperature difference gradually increased with the increase of the setting temperature. It should be noted that the surface temperature of the graphite plate detected by the IR thermal camera was slightly lower than the setting, which is related to the IR emissivity of the graphite coating. In particular, when the temperature of the heating plate was set to 100 °C, the surface temperature of the MG-C4/CF captured by the IR camera was only 60.5 °C, which can be reduced by 26.4 °C compared to that of the original CF (86.9 °C) (Fig. 7b). Figure 7c illustrates the proposed mechanism of IR thermal camouflage of MG-C4/CF. The heat generated by the body's metabolism is continuously radiated through the skin to the external space environment. While encountered with MG-C4/CF, the assembled MXene on the fabric surface possesses a low IR emissivity that will prevent the diffusion process of thermal radiation, thus giving the fabric excellent thermal camouflage abilities.

The MG-C4/CF has the characteristics of low IR emissivity properties while retaining the inherent softness, bendability and breathability of the fabric, making it meet the conditions for free and flexible wear on the body surface. From Fig. 7d, the surface temperature of the MG-C4/CF covered body upper arm is close to the ambient temperature and well below the skin surface temperature, both indoors and outdoors. Besides, MG-C4/CF covered directly on the bare palm and wrist captured radiation temperatures that differed from the ambient temperature by only 1.4–1.5 °C, a value of 8.1–8.6 °C when MG-C4/CF was not covered (Fig. 7e, f). This indicates that MG-C4/CF are promising candidates for man-at-arms uniforms that can play a role in protecting soldiers against enemy detection.

Conclusions

In this work, a conductive network with a layer-by-layer assembled 'wire-surface' structure was constructed on the cotton fabric surface for the preparation wearable multifunctional personal protective textiles. Guided by an easy-to-operate, mass-manufacturable spraying strategy, CNTs and MG dispersions were deposited in an alternating orderly assembly on the cotton surface, and the assembled fabric achieved a low resistance value of 24.6 Ω. The assembly fabric is breathable and moisture permeable, bendable and flexible, maintaining their original conductivity after 1 000 cycles of bending and 60 days of nature storage. By taking advantage of the excellent conductivity of the assembled fabric, it is possible to achieve high EMI shielding effectiveness (35 dB) and outstanding IR thermal camouflage performance. Besides, low-radiation heating, *Joule* heating and solar heating are integrated to the MG-C4/CF, ensuring that it might respond to the heating needs of complex scenarios and achieve efficient utilization of energy. Based on its green manufacturing

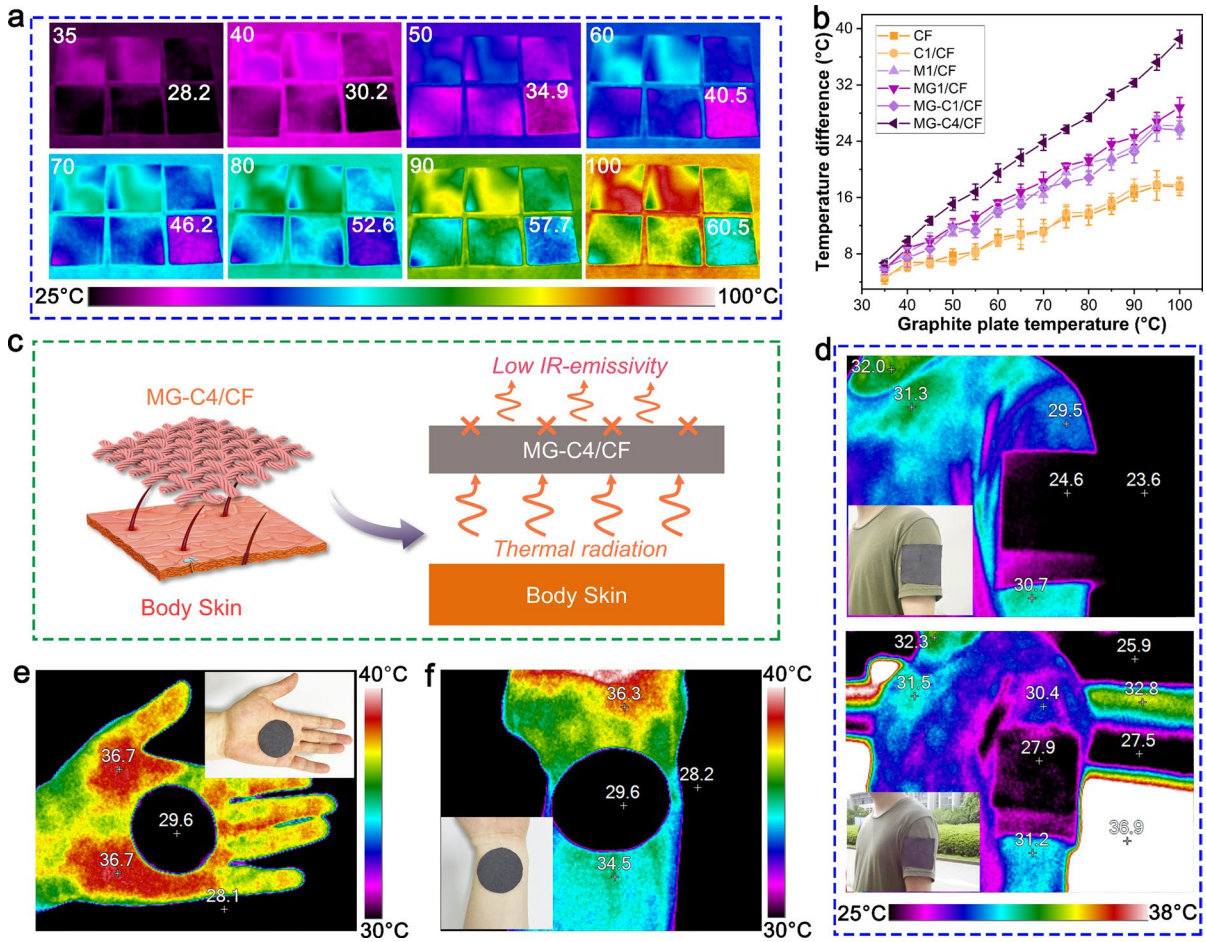

Fig. 7 **a** Infrared (IR) thermal images of fabrics on graphite heating plate substrates at different temperatures (the top row, from left to right, CF, C1/CF and M1/CF, the bottom row, from left to right, MG1/CF, MG-C1/CF and MG-C4/CF.). **b** Difference in IR detection temperature between the fabrics and graphite heating plate. **c** Schematic diagram of the IR thermal camouflage mechanism of MG-C4/CF. IR thermal camouflage effect of the **d** upper arm indoors and outdoors, **e** palm, and **f** wrist covered by MG-C4/CF

process, good durability and excellent comfort, the assembled fabric of MG-C4/CF will be a promising candidate for manufacturing multifunctional personal protective garments.

Acknowledgments Financial support from the Six Talent Peaks Projects in Jiangsu Province (XCL-133), the National Natural Science Foundation of China (22109054) and Postgraduate Research & Practice Innovation Program of Jiangsu Province (KYCX22_2333) are gratefully acknowledged.

Author contributions BY: Conceptualization, Methodology, Software, Formal analysis, Investigation, Writing-original draft. YG: Methodology, Software, Formal analysis, Investigation. BF: Methodology, Investigation. MZ: Investigation, Formal analysis, Supervision, Methodology. YL: Supervision, Methodology. YY: Supervision, Methodology. BX: Supervision, Methodology. QW: Supervision, Methodology. PW: Conceptualization, Methodology, Validation, Resources, Writing-review & editing, Project administration, Funding acquisition. All authors reviewed the manuscript.

Funding This work was financially supported by the Six Talent Peaks Projects in Jiangsu Province (XCL-133), the National Natural Science Foundation of China (22109054) and Postgraduate Research & Practice Innovation Program of Jiangsu Province (KYCX22_2333).

Data availability The data and materials that support the findings of this study are available from the corresponding author upon reasonable request.

Declarations

Competing interests The authors declare no competing interests.

Ethics approval and consent to participate All authors have consented to participate on the manuscript.

Consent for publication All authors have approved the final version of the manuscript.

References

Alhabeb M, Maleski K, Anasori B, Lelyukh P, Clark L, Sin S, Gogotsi Y (2017) Guidelines for synthesis and processing of two-dimensional titanium carbide ($Ti_3C_2T_x$ MXene). Chem Mater 29(18):7633–7644. https://doi.org/10.1021/acs.chemmater.7b02847

Allison L, Hoxie S, Andrew TL (2017) Towards seamlessly-integrated textile electronics: methods to coat fabrics and fibers with conducting polymers for electronic applications. Chem Commun 53(53):7182–7193. https://doi.org/10.1039/C7CC02592K

Cai G, Yang M, Pan J, Cheng D, Xia Z, Wang X, Tang B (2018) Large-scale production of highly stretchable CNT/cotton/spandex composite yarn for wearable applications. ACS Appl Mater Interfaces 10(38):32726–32735. https://doi.org/10.1021/acsami.8b11885

Cao R, Pu X, Du X, Yang W, Wang J, Guo H, Zhao S, Yuan Z, Zhang C, Li C, Wang ZL (2018) Screen-printed washable electronic textiles as self-powered touch/gesture tribosensors for intelligent human-machine interaction. ACS Nano 12(6):5190–5196. https://doi.org/10.1021/acsnano.8b02477

Cui Y, Jiang Z, Zheng G, Wang W, Zhou M, Wang P, Yu Y, Wang Q (2022) Green preparation of PEDOT-based composites with outstanding electrothermal heating and durable rapid-response sensing performance for smart healthcare textiles. Chem Eng J 446:137189. https://doi.org/10.1016/j.cej.2022.137189

Gao M, Zhu L, Peh CK, Ho GW (2019) Solar absorber material and system designs for photothermal water vaporization towards clean water and energy production. Energy Environ Sci 12(3):841–864. https://doi.org/10.1039/C8EE01146J

Ghos S, Mondal S, Ganguly S, Remanan S, Singha N, Das NC (2018) Carbon nanostructures based mechanically robust conducting cotton fabric for improved electromagnetic interference shielding. Fiber Polym 19:1064–1073. https://doi.org/10.1007/s12221-018-7995-4

Ghosh S, Greenfeld I, Wagner HD (2023) CNT coating and anchoring beads enhance interfacial adhesion in fiber composites. Compos Part A-Appl S 167:107427. https://doi.org/10.1016/j.compositesa.2023.107427

Guo Z, Sun C, Wang J, Cai Z, Ge F (2021) High-performance laminated fabric with enhanced photothermal conversion and joule heating effect for personal thermal management. ACS Appl Mater Interfaces 13(7):8851–8862. https://doi.org/10.1021/acsami.0c23123

Guo Y, Tian Q, Wang T, Wang S, He X, Ji L (2023) Silver nanoparticles decorated meta-aramid nanofibrous membrane with advantageous properties for high-performance flexible pressure sensor. J Colloid Interface Sci 629:535–545. https://doi.org/10.1016/j.jcis.2022.09.096

Gupta R, Rao KDM, Kiruthika S, Kulkarni GU (2016) Visibly transparent heaters. ACS Appl Mater Interfaces 8(20):12559–12575. https://doi.org/10.1021/acsami.5b11026

Heo JS, Eom J, Kim YH, Park SK (2018) Recent progress of textile-based wearable electronics: a comprehensive review of materials, devices, and applications. Small 14(3):1703034. https://doi.org/10.1002/smll.201703034

Hsu PC, Liu X, Liu C, Xie X, Lee HR, Welch AJ, Zhao T, Cui Y (2015) Personal thermal management by metallic nanowire-coated textile. Nano Lett 15(1):365–371. https://doi.org/10.1021/nl5036572

Iqbal A, Shahzad F, Hantanasirisakul K, Kim MK, Kwon J, Hong J, Kim H, Kim D, Gogotsi Y, Koo CM (2020) Anomalous absorption of electromagnetic waves by 2D transition metal carbonitride Ti_3CNT_x (MXene). Science 369(6502):446–450. https://doi.org/10.1126/science.aba7977

Ji Y, Li Y, Chen G, Xing T (2017) Fire-resistant and highly electrically conductive silk fabrics fabricated with reduced graphene oxide via dry-coating. Mater Des 133:528–535. https://doi.org/10.1016/j.matdes.2017.08.006

Jin H, Nayeem M, Lee S, Matsuhisa N, Inoue D, Yokota T, Hashizume D, Someya T (2019) Highly durable nanofiber-reinforced elastic conductors for skin-tight electronic textiles. ACS Nano 13(7):7905–7912. https://doi.org/10.1021/acsnano.9b02297

Jose S, Prakash A, Laha S, Natarajan S, Reddy ML (2014) Green colored nano-pigments derived from Y_2BaCuO_5: NIR reflective coatings. Dyes Pigm 107:118–126. https://doi.org/10.1016/j.dyepig.2014.03.025

Lee Y, Le VT, Kim JG, Kang H, Kim ES, Ahn SE, Suh D (2018) Versatile, high-power, flexible, stretchable carbon nanotube sheet heating elements tolerant to mechanical damage and severe deformation. Adv Funct Mater 28(8):1706007. https://doi.org/10.1002/adfm.201706007

Lee GS, Yun T, Kim H, Kim IH, Choi J, Lee SH, Lee HJ, Hwang HS, Kim JG, Kim DW, Lee HM, Koo CM, Kim SO (2020) Mussel inspired highly aligned $Ti_3C_2T_x$ MXene film with synergistic enhancement of mechanical strength and ambient stability. ACS Nano 14(9):11722–11732. https://doi.org/10.1021/acsnano.0c04411

Li R, Zhang L, Shi L, Wang P (2017) MXene Ti_3C_2: an effective 2D light-to-heat conversion material. ACS Nano 11(4):3752–3759. https://doi.org/10.1021/acsnano.6b08415

Li BM, Yildiz O, Mills AC, Flewwellin TJ, Bradford PD, Jur JS (2020) Iron-on carbon nanotube (CNT) thin films for biosensing E-textile applications. Carbon 168:673–683. https://doi.org/10.1016/j.carbon.2020.06.057

Li L, Shi M, Liu X, Jin X, Cao Y, Yang Y, Wang W, Wang J (2021) Ultrathin titanium carbide (MXene) films for high-temperature thermal camouflage. Adv Funct Mater 31(35):2101381. https://doi.org/10.1002/adfm.202101381

Li H, Pan Y, Du Z (2022) Self-reduction assisted MXene/silver composite Tencel cellulose-based fabric with

electrothermal conversion and NIR photothermal actuation. Cellulose 29(15):8427–8441. https://doi.org/10.1007/s10570-022-04766-5

Lipatov A, Alhabeb M, Lukatskaya MR, Boson A, Gogotsi Y, Sinitskii A (2016) Effect of synthesis on quality, electronic properties and environmental stability of individual monolayer Ti_3C_2 MXene flakes. Adv Energy Mater 2(12):1600255. https://doi.org/10.1002/aelm.201600255

Liu Q, Huang J, Zhang J, Hong Y, Wan Y, Wang Q, Gong M, Wu Z, Guo CF (2018) Thermal, waterproof, breathable, and antibacterial cloth with a nanoporous structure. ACS Appl Mater Interfaces 10(2):2026–2032. https://doi.org/10.1021/acsami.7b16422

Lucente-Schultz RM, Moore VC, Leonard AD, Price BK, Kosynkin DV, Lu M, Partha R, Conyers JL, Tour JM (2009) Antioxidant single-walled carbon nanotubes. J Am Chem Soc 131(11):3934–3941. https://doi.org/10.1021/ja805721p

Naguib M, Kurtoglu M, Presser V, Lu J, Niu J, Heon M, Hultman L, Gogotsi Y, Barsoum MW (2011) Two-dimensional nanocrystals produced by exfoliation of Ti_3AlC_2. Adv Mater 23(37):4248–4253. https://doi.org/10.1002/adma.201102306

Rajavel K, Yu X, Zhu P, Hu Y, Sun R, Wong C (2021) Investigation on the structural quality dependent electromagnetic interference shielding performance of few-layer and lamellar Nb_2CT_x MXene nanostructures. J Alloys Compd 877:160235. https://doi.org/10.1016/j.jallcom.2021.160235

Salihoglu O, Uzlu HB, Yakar O, Aas S, Kakenov O, Balci N, Olcum S, Süzer S, Kocabas C (2018) Graphene-based adaptive thermal camouflage. Nano Lett 18(7):4541–4548. https://doi.org/10.1021/acs.nanolett.8b01746

Sarycheva A, Gogotsi Y (2020) Raman spectroscopy analysis of the structure and surface chemistry of $Ti_3C_2T_x$ MXene. Chem Mater 32(8):3480–3488. https://doi.org/10.1021/acs.chemmater.0c00359

Su Z, Yang H, Wang G, Zhang Y, Zhang J, Lin J, Jia D, Wang H, Lu Z, Hu P (2023) Transparent and high-performance electromagnetic interference shielding composite film based on single-crystal graphene/hexagonal boron nitride heterostructure. J Colloid Interface Sci 640:610–618. https://doi.org/10.1016/j.jcis.2023.02.115

Takei K, Honda W, Harada S, Arie T, Akita S (2015) Toward flexible and wearable human-interactive health-monitoring devices. Adv Healthc Mater 4(4):487–500. https://doi.org/10.1002/adhm.201400546

Wang Q, Zhang H, Liu J, Zhao S, Xie X, Liu L, Yang R, Koratkar N, Yu ZZ (2019) Multifunctional and water-resistant MXene-decorated polyester textiles with outstanding electromagnetic interference shielding and joule heating performances. Adv Funct Mater 29(7):1806819. https://doi.org/10.1002/adfm.201806819

Wang X, Lei Z, Ma X, He G, Xu T, Tan J, Wang L, Zhang X, Qu L, Zhang X (2022) A lightweight MXene-coated nonwoven fabric with excellent flame retardancy, EMI shielding, and electrothermal/photothermal conversion for wearable heater. Chem Eng J 430:132605. https://doi.org/10.1016/j.cej.2021.132605

Xu H, Yin X, Li X, Li M, Liang S, Zhang L, Cheng L (2019) Lightweight Ti_2CT_x MXene/poly (vinyl alcohol) composite foams for electromagnetic wave shielding with absorption-dominated feature. ACS Appl Mater Interfaces 11(10):10198–10207. https://doi.org/10.1021/acsami.8b21671

Yan B, Zhou M, Liao X, Wang P, Yu Y, Yuan J, Wang Q (2021) Developing a multifunctional silk fabric with dual-driven heating and rapid photothermal antibacterial abilities using high-yield MXene dispersions. ACS Appl Mater Interfaces 13(36):43414–43425. https://doi.org/10.1021/acsami.1c12915

Yan B, Zhou M, Yu Y, Xu B, Cui L, Wang Q, Wang P (2022) Orderly self-stacking a sigh-stability coating of MXene@polydopamine hybrid onto textiles for multifunctional personal thermal management. Compos Part A Appl Sci Manuf 160:107038. https://doi.org/10.1016/j.compositesa.2022.107038

Yan B, Huang S, Ren Y, Zhou M, Yu Y, Xu B, Cui L, Wang Q, Wang P (2023) HRP-catalyzed grafting of MXene@PGA to silk fibers for visualization of dual-driven heating smart textile. Int J Biol Macromol 226:1141–1153. https://doi.org/10.1016/j.ijbiomac.2022.11.228

Yang Z, Pang Y, Han X, Yang Y, Ling J, Jian M, Zhang Y, Yang Y, Ren TL (2018) Graphene textile strain sensor with negative resistance variation for human motion detection. ACS Nano 12(9):9134–9141. https://doi.org/10.1021/acsnano.8b03391

Yao D, Tang Z, Zhang L, Li R, Zhang Y, Zeng H, Du D, Ouyang J (2021) Gas-permeable and highly sensitive, washable and wearable strain sensors based on graphene/carbon nanotubes hybrids e-textile. Compos Part A Appl Sci 149:106556. https://doi.org/10.1016/j.compositesa.2021.106556

Yao Y, Jin S, Wang M, Gao F, Xu B, Lv X, Shu Q (2022) MXene hybrid polyvinyl alcohol flexible composite films for electromagnetic interference shielding. Appl Surf Sci 578:152007. https://doi.org/10.1016/j.apsusc.2021.152007

Yin G, Wang Y, Wang W, Yu D (2020) Multilayer structured PANI/MXene/CF fabric for electromagnetic interference shielding constructed by layer-by-layer strategy. Colloid Surf A Physiochem Eng 601:125047. https://doi.org/10.1016/j.colsurfa.2020.125047

Zhang Q, Liu D, Pan W, Pei H, Wang K, Xu S, Liu Y, Cao S (2022) Flexible stretchable electrothermally/photothermally dual-driven heaters from nano-embedded hierarchical Cu_xS-coated PET fabrics for all-weather wearable thermal management. J Colloid Interface Sci 624:564–578. https://doi.org/10.1016/j.jcis.2022.05.159

Zhao Y, Wang J, Li Z, Zhang X, Tian M, Zhang X, Liu X, Qu L, Zhu S (2020) Washable, durable and flame retardant conductive textiles based on reduced graphene oxide modification. Cellulose 27:1763–1771. https://doi.org/10.1007/s10570-019-02884-1